Molecular Cancer

RESEARCH

Open Access

Chimeric antigen receptor macrophages targeting c-MET(CAR-M-c-MET) inhibit pancreatic cancer progression and improve cytotoxic chemotherapeutic efficacy

Huaijin Zheng[1†], Xinzhe Yang[3†], Nan Huang[1], Shangqin Yuan[1], Jiayi Li[1], Xudong Liu[2], Qing Jiang[3], Shanshan Wu[3], Yue Ju[4], Jorg Kleeff[5], Xiushan Yin[3,4*], Quan Liao[1*], Qiaofei Liu[1*] and Yupei Zhao[1*]

Abstract

Background Pancreatic ductal adenocarcinoma (PDAC) is one of the most malignant tumors. Macrophages are abundant in the tumor microenvironment, making them an attractive target for therapeutic intervention. While current immunotherapies, including immune checkpoint inhibition (ICI) and chimeric antigen receptor T (CAR-T) cells, have shown limited efficacy in pancreatic cancer, a novel approach involving chimeric antigen receptor macrophages (CAR-M) has, although promising, not been explored in pancreatic cancer. In this study, we first investigated the role of CAR-M cells targeting c-MET in pancreatic cancer.

Methods The effectiveness and rationality of c-MET as a target for CAR-M in pancreatic cancer were validated through bioinformatic analyses and immunohistochemical staining of samples from pancreatic cancer patients. We utilized flow cytometry and bioluminescence detection methods to demonstrate the specific binding and phagocytic killing effect of CAR-M on pancreatic cancer cells. Additionally, we observed the process of CAR-M engulfing pancreatic cancer cells using confocal microscopy and a long-term fluorescence live cell imaging system. In an in situ tumor model transplanted into NOD/SCID mice, we administered intraperitoneal injections of CAR-M to confirm its inhibitory function on pancreatic cancer. Furthermore, we validated these findings in human monocyte-derived macrophages (hMDM).

Results Bioinformatics and tumor tissue microarray analyses revealed significantly higher expression levels of c-MET in tumor tissues, compared to the paired peritumoral tissues, and higher c-MET expression correlated with worse patient survival. CAR-M cells were engineered using human monocytic THP-1 cell line and hMDM targeting c-MET (CAR-M-c-MET). The CAR-M-c-MET cells demonstrated highly specific binding to pancreatic cancer cells and exhibited

[†]Zhen HJ and Yang XZ were the co-first authors.

*Correspondence:
Xiushan Yin
xiushanyin@gmail.com
Quan Liao
pumclq@126.com
Qiaofei Liu
qfliu@aliyun.com
Yupei Zhao
zhao8028@263.net
Full list of author information is available at the end of the article

more phagocytosis and killing abilities than the pro-inflammatory polarized control macrophages. In addition, CAR-M-c-MET cells synergized with various cytotoxic chemotherapeutic drugs. In a NOD/SCID murine model, intraperitoneally injected CAR-M-c-MET cells rapidly migrated to tumor tissue and substantially inhibited tumor growth, which did not lead to obvious side effects. Cytokine arrays and mRNA sequencing showed that CAR-M-c-MET produced higher levels of immune activators than control macrophages.

Conclusions This study provides compelling evidence for the safety and efficacy of CAR-M therapy in treating pancreatic cancer. The results demonstrate that CAR-M-c-MET significantly suppresses pancreatic cancer progression and enhances the effectiveness of cytotoxic chemotherapy. Remarkably, no discernible side effects occur. Further clinical trials are warranted in human pancreatic cancer patients.

Keywords Chimeric antigen receptor macrophage, Pancreatic cancer, c-MET, Chemotherapy

Introduction

Pancreatic cancer remains a formidable adversary, with a rising global incidence [1]. While advances in pancreatic surgery and cytotoxic chemotherapy have led to a higher percentage of patients being safely resected and improved survival rates, the 5-year overall survival for all patients remains below 10%, and even for localized pancreatic cancer without lymph node metastasis remains at only around 40–45%. Additionally, the response rate to the standard four-drug combined regimen (Folfirinox) is only up to one-third [2–4]. New therapy modalities are urgently needed to improve further this poor prognosis and therapy response [5]. Pancreatic cancer is characterized by a dense stromal reaction in the tumor microenvironment with immune cell infiltration, although with a relative lack of effector T cells and anti-tumor macrophages [6]. Nonetheless, immunotherapies for pancreatic cancer have been analyzed in preclinical models and clinical trials. Immune checkpoint inhibitors (ICI) and chimeric antigen receptor T cells (CAR-T) are two milestones of clinical immunotherapy. However, both exhibited minimal efficacy in pancreatic cancer [7]. Macrophages are the most predominant immune cells in pancreatic cancer tissue [8]. The function of tumor-associated macrophages (TAMs) is multifaceted. While macrophages possess potent phagocytic abilities and can modulate the immune response, they also contribute to tumor progression and chemoresistance through various inflammatory processes [6, 9–11]. Immunotherapies targeting TAMs have gained attention during the last decade [12, 13]. Compared to CAR-T, chimeric antigen receptor macrophages (CAR-M) have specific advantages for solid tumors due to their tumor infiltration capacities, the ability of phagocytosis, and low risk of graft versus host diseases (GVHD) [7, 14]. However, the roles of CAR-M have not been investigated in pancreatic cancer.

C-MET is a tyrosine kinase receptor belonging to the MET family with its ligand hepatocyte growth factor (HGF). Aberrant HGF/c-MET activation in pancreatic cancer promotes tumor development and progression by stimulating PI3K/AKT, Ras/MAPK, JAK/STAT, and Wnt/β-catenin signaling pathways [15]. Several preclinical studies reported that c-MET inhibition reduces metastatic spread and enhances chemotherapy efficacies in pancreatic cancer [16, 17]. This study explored the safety and effectiveness of CAR-M targeting c-MET (CAR-M-c-MET) in pancreatic cancer. It is shown that CAR-M-c-MET is a safe and effective new immunotherapy avenue to target pancreatic cancer and improve cytotoxic chemotherapeutic efficacy.

Methods

Bioinformatic analysis

Data were acquired from the National Cancer Institute Genomic Data Commons database via The Cancer Genome Atlas (TCGA) pancreatic adenocarcinoma (PAAD) dataset. Specifically, gene expression data for.

c-MET were extracted from TCGA-PAAD. Demographic information, treatment modalities, clinical endpoints, and follow-up data pertaining to patients were also retrieved from the TCGA-PAAD repository. To stratify patients based on c-MET expression levels, the median expression value was employed as the cutoff threshold, thereby segregating patients into high and low-expression groups. Kaplan–Meier survival analysis was subsequently carried out to assess the prognostic significance of c-MET expression. A threshold of $p < 0.05$ was applied to define statistical significance in survival outcomes between the aforementioned groups. This study adheres to the guidelines and protocols established by the TCGA and the National Cancer Institute, ensuring rigor and reproducibility of data analysis.

Tissue microarray analysis and immunohistochemistry (IHC)staining

Tissue microarray sections were constructed, each measuring 4 μm in thickness, encompassing 90 pairs of pancreatic ductal adenocarcinoma (PDAC) samples and adjacent peritumoral pancreatic tissues (Shanghai Outdo Biotech Co. Ltd). The relevant demographic data, tumor

pathological grading, clinical stage of PDAC, and survival information were obtained through follow-up. The Institutional Review Board approved the construction and use of this tissue microarray (SHYJS-CP-1901011, Shanghai Outdo Biotech Co. Ltd). Immunohistochemical (IHC) analysis was conducted using a c-MET monoclonal antibody (dilution: 1:500, 25,869–1-AP, Proteintech, Wuhan, China), with overnight incubation at 4 °C. Slides were analyzed via microscopy (Nikon ECLIPSETs2R, Japan). The details of the clinicopathological characteristics of the patient cohort are presented in Table S1.

The inclusion criteria for further analysis were radical resection for resectable pancreatic ductal adenocarcinoma patients, R0 resection with cancer cell-free margins (0 mm rule), and survival time longer than three months after surgery.

For staining evaluation of c-MET, the ratio of positive cancer cells was classified into five grades (0: 0–5%; 1: 6%-25%; 2: 26%-50%; 3: 51% to 75%; 4: 76% to 100%), and the staining intensity was classified into four grades (0–3). The final score was the value of the ratio × the value of the staining intensity. The final staining score of 0–4, 5–8, and 9–12 was defined to be negative/weak, moderate, and strong expression, respectively. The X-TILE program(https://x-tile.software.informer.com/) was used to determine the optimal cutoff value of the staining score of c-MET to predict the survival of the patients [8].

Cell lines, primary human monocytes, and culture conditions

The pancreatic cancer cell lines PANC1, BxPC-3, AsPC-1, PATU8988T, and MIA PaCa-2, as well as the human monocyte cell line THP-1, were all obtained from the National Infrastructure of Cell Line Resource of the Chinese Academy of Medical Sciences and preserved in the Laboratory of General Surgery at Peking Union Medical College Hospital. Cells were cultured in DMEM (C11995500BT, Gibco, NewYork, USA) and RPMI-1640 (C22400500BT, Gibco, NewYork, USA) media with 10% fetal bovine serum (FBS, 04–001-1A, Biological Industries, Israel) and 1% penicillin & streptomycin (03–031-1B, Biological Industries, Israel) and were grown in a cell incubator (37 °C with 5% CO2). Human gastric cancer cell N87 was derived from Shanghai Binsui Biotechnology Co., Ltd. and stored in the Applied Biology Research Laboratory of Shenyang University of Chemical Technology. The cells were cultured in DMEM (Corning) medium containing 10% fetal bovine serum (FND500, Excell, Australia)and 1%penicillin and streptomycin(PS2004HY, TBDScience, China). THP-1 was induced to adhere by employing a final concentration of 100 ng/ml phorbol 12-myristate 13-acetate (PMA) (P8139, Sigma-Aldrich, USA). After 24 h of induction, the cells adhered to become primary macrophages (M0). 20 ng/ml IFN-γ (GMP-CI57, Novoprotein, China) and 100 ng/ml LPS (L8880, Solarbio, China) were added to the culture medium. After 24 h, the cells were induced to a pro-inflammatory phenotype [18]. Preparation of BMDM: C57 mice were dislocated and sacrificed to take the tibia and femur of the hind limbs, the syringe aspirated DMEM medium to blow the bone marrow cells in the bone cavity into a 50 ml centrifuge tube, 700 g centrifugation for 5 min, after discarding the supernatant, 3 ml of erythrocyte lysate was added for 3 min, then 30 ml of PBS was added, 700 g centrifugation after passing through the 100 μm cell sieve for 5 min to obtain bone marrow cell pellet, and supplemented with 10% FBS (FND500, Excell, Australia) and Induce culture in DMEM medium (Corning) at 100 μg/ml penicillin–streptomycin (PS2004HY, TBDScience, China) and 10 ng/mI M-CSF (AF-300–25, PeproTech, United States) for 5 days to obtain mouse primary bone marrow-derived macrophages (BMDMs). Finally, CAR-M is obtained 48 h after chimeric antigen receptor (CAR) infection. All of these cells were cultured at 37 °C and 5% CO2.

Peripheral blood mononuclear cells (PBMC) were isolated by density gradient centrifugation. First, approximately 70 ml of peripheral blood from donors was mixed with saline at a nearly 1:1 ratio, a step that could be performed in multiple 50 ml centrifuge tubes. Then, the mixture was gently added from the edge of the centrifuge tube to a high-efficiency centrifuge tube with lymphocyte isolate and centrifuged at 600 g for 20 min. Next, the plasma was discarded, and the buffy coat was transferred to a new 50 ml centrifuge tube and centrifuged at a rate of 700 g for 5 min. Subsequently, saline was added to the cell pellet for re-suspension and centrifuged again at 700 g for 5 min. After repeating this washing step, the cells were counted using a hemocytometer. Following this, CD14 + monocytes were isolated from PBMC by positive selection of magnetic beads (No.130–050-201-CD14, Miltenyi Biotech, Germany) and induced by culture for five days in RPMI 1640 medium (Corning) supplemented with 10% FBS (FND500, Excell, China), and 100 μg/ml penicillin–streptomycin (PS2004HY, TBDScience, China) and 10 ng/ml GM-CSF (300–03, PeproTech, USA) to obtain human monocyte-derived macrophages (hMDM). Finally, CAR-M was obtained 48 h after chimeric antigen receptor (CAR) infection. All these cells were cultured at 37℃ and 5% CO2.

Flow cytometry (FCM)

Cells were harvested through standard digestion, centrifugation, and resuspension in the cell staining buffer. The cell density was adjusted to $3–8 \times 10^5$ cells/ml, and each group received 1 ml of the cell suspension. For human

cells, Fc receptors were blocked using 5 µl TruStain FcXTM (156,603, BioLegend, USA) per 100 µl of cell suspension, followed by 10 min incubation at room temperature. After centrifugation, cells were incubated with an appropriate primary antibody on ice for 30 min. Following centrifugation and washing, cells were resuspended. After a 5 min incubation on ice, the samples were ready for flow cytometry analysis. Flow cytometry was performed using the FITC channel for cells expressing GFP fluorescent protein and the PE-mCherry channel for cells expressing mCherry fluorescent protein.

THP-1 cells were incubated with his-tag hu-c-METrecombinant protein (2 µg/ml) (10,692-H08H, SinoBiological, China) at 37° C for 2 h, then blocked by TruStain FcXTM, and then incubated with PE/Cy7 anti-his tag flow antibody (352,620, Biolegend, USA) for 30 min. Subsequently, the binding efficiency of the target protein was detected using an LSRFortessa™ flow cytometer (BD, USA), and analysis was performed using FlowJo10.10 software. The antibodies used were FITC anti-human c-MET (11,885,842, Biolegend, USA), PE/Cy7 anti-his tag (352,620, Biolegend, USA), and Human TruStain FcXTM (422,301, Biolegend, USA).

Her2 antigen detection

Count 1×10^6 N87 and BxPC3 cells, centrifuge at 1000 rpm for 5 min, resuspend in 100 µl PBS, then add 10 µl HER2-FITC (BMS120FI, Invitrogen, USA), and incubate in the dark at 4 °C for 30 min.

Construction of CARs and cell transfection

The CAR construct comprises the CD8α signal peptide, the c-MET single-chain variable fragment (scFv) sequence (targeting human and murine Homologous sequence of c-MET), the CD8α hinge region, the Fc receptor γ (FcRγ) signaling activation domain, and the CD19 phosphoinositide 3-kinase (PI3K) recruitment domain, concomitantly linked with an EGFP sequence via a T2A sequence. The CAR plasmid and lentiviral vector expressing the CAR plasmid were synthesized through commissioning to Shanghai Genechem Co., Ltd (GIEL0320172). A patent has been applied before submitting this paper. Therefore, the details of the CAR remain confidential. The THP-1 cell line was transfected with this lentivirus at a multiplicity of infection (MOI) of 30. Seventy-two hours after transfection, the CAR-M-c-MET THP-1 cells expressing the GFP fluorescent tag were sorted by flow cytometry, purified, and expanded. The THP-1 cell line was transfected with lentivirus containing only a GFP fluorescent tag or luciferase at an MOI of 30, and BxPC-3 cells were transfected with lentivirus containing only a mCherry fluorescent tag and luciferase at an MOI of 10 to construct NC THP-1, NC THP-1 luci + control macrophages, BxPC-3 mCherry +, and BxPC-3 luci + target cells.

To prepare CAR-M-c-MET hMDM, CAR gene constructs were integrated into an adenovirus-modified vector based on the Ad5f35 adenovirus backbone, in which the CAR gene constructs include the CD8 signal peptide, (GGGGS)3 linker, CD8 hinge, and CD8 transmembrane structural domains, as well as the CD19 or CD3ζ intracellular structural domains, the expression of which was regulated by the EF1α promoter. Adenovirus preparation, amplification, concentration, and purification were performed in 293A cells using standard techniques. Adenovirus titers were determined using the Clontech Adenovirus Rapid Titer Kit(632,250, Clontech, USA), and their expression was confirmed in human macrophages. The MOI was maintained at 2,000 ifu and ifu was calculated based on the average number of positive cells per unit dilution according to manufacturer's instructions.

In vitro *co-culture experiments*

The induced pro-inflammatory polarized CAR THP-1 and NC THP-1, BxPC-3 mCherry + or BxPC-3 luci + were digested, mixed, and spread into 6-well plates according to different effector/target (E:T) ratios. The co-culture system was digested at various time points and then detected by FCM, or the fluorescein signal of the co-culture system was detected by IVIS Lumina III (PerkinElmer, USA) at different time points and quantified by Living Image®.

Lactate dehydrogenase (LDH) assays

The supernatant from co-culture systems was collected and subjected to LDH cytotoxicity assessment using the LDH Cytotoxicity Assay Kit (C0016, Beyotime, China). For maximum LDH activity, the LDH release reagent provided in the kit was added at a volume equivalent to 10% of the original culture volume. Following the addition of the LDH release reagent, gentle agitation was applied to ensure thorough mixing, followed by continued incubation in the cell culture chamber. After 1 h, the cell culture plate was centrifuged at 400 g for 5 min using a multi-well plate centrifuge. Subsequently, 120 µl of the supernatant from each well was transferred to the corresponding wells of a new 96-well plate. To each well, 60 µl of LDH detection working solution, prepared according to the manufacturer's instructions, was added, followed by thorough mixing and incubation at room temperature (approximately 25 °C) in the dark for 30 min. Absorbance was measured at 490 nm, with a reference wavelength of 600 nm for dual-wavelength determination. The obtained absorbance readings for each group were background-corrected by subtracting the absorbance of blank control wells.

LDH release rate (%) was calculated using the formula: LDH release rate (%) = (absorbance of treated samples—absorbance of sample control wells) / (absorbance representing maximum LDH activity wells—absorbance of sample control wells) × 100%.

Confocal microscopy photography and live cell high-speed laser confocal real-time imaging Following a 1:1 co-culture of CAR THP-1 or NC THP-1, hMDM-CAR or hMDM-Adv-mCherry with BxPC-3 mCherry + cells, the co-culture system was fixed with 4% (w/vol) paraformaldehyde after 24 h. Subsequent imaging was conducted using a confocal microscope(Nikon AXR, Japan), and images were subjected to analysis using ImageJ software. Additionally, a PerkinElmer UltraVIEW VoX high-speed laser scanning confocal real-time imaging system was employed for continuous imaging over a 24-h period.

Combination of cytotoxic chemotherapy and CAR-M-c-MET

Thirty thousand BxPC-3 luci + cells were seeded into each well of a 48-well plate and treated with gemcitabine, 5-fluorouracil, irinotecan, and oxaliplatin chemotherapy agents(10 μM), respectively, with three replicates per treatment group. Following 24 h of incubation, the culture medium was replaced, and a specific number of CAR THP-1 or NC THP-1 cells were added at various E:T ratios. Co-cultures were maintained for an additional 24 h before bioluminescence fluorescence signal detection and LDH assessment of the supernatants.

RNA-seq

Following a 48 h co-culture of CAR THP-1 or NC THP-1, hMDM-CAR, hMDM-Adv-mCherry, or hMDM-UTD with BxPC-3 cells, macrophages were isolated from the co-culture system using flow cytometry-based cell sorting. After centrifugation, TRIzol reagent (Takara, Cat#9108) was added to the pellet for RNA extraction, with three replicates per group, for subsequent sequencing analysis (Shanghai Boitechonology Corporation, Shanghai, China).

(1) Library construction for RNA-sequencing procedures:

Total RNA was isolated using RNeasy Mini Kit (Qiagen). Paired-end libraries were synthesized by using the TruSeq® RNA Sample Preparation Kit (Illumina, USA) following TruSeq® RNA Sample Preparation Guide. Briefly, the poly-A containing mRNA molecules were purified using poly-T oligo-attached magnetic beads. Following purification, the mRNA is fragmented into small pieces using divalent cations under 94 °C for 8 min. The cleaved RNA fragments are copied into first strand cDNA using reverse transcriptase and random primers. This is followed by second strand cDNA synthesis using DNA Polymerase I and RNase H. These cDNA fragments then go through an end repair process, the addition of a single 'A' base, and then ligation of the adapters. The products are then purified and enriched with PCR to create the final cDNA library. Purified libraries were quantified by Qubit® 2.0 Fluorometer (Life Technologies, USA) and validated by Agilent 2100 bioanalyzer (Agilent Technologies, USA) to confirm the insert size and calculate the mole concentration. Cluster was generated by cBot with the library diluted to 10 pM and were then sequenced on the Illumina HiSeq Xten (Illumina, USA). The library construction and sequencing were performed at Shanghai Biotechnology Corporation.

(2) Data analysis for gene expression:

Sequencing raw reads were preprocessed by filtering out rRNA reads, sequencing adapters, short fragment reads and other low-quality reads. We used Hisat2 (version:2.0.4) to map the cleaned reads to the human hg38 reference genome with two mismatches. After genome mapping, Stringtie(version:1.3.0) was run with a reference annotation to generate FPKM values for known gene models. Differentially expressed genes were identified using edgeR. The p-value significance threshold in multiple tests was set by the false discovery rate (FDR). The fold-changes were also estimated according to the FPKM in each sample. The differentially expressed genes were selected using the following filter criteria: FDR ≤ 0.05 and fold-change ≥ 2.

RT-qPCR

NC THP-1 and CAR THP-1 was co-cultured with BxPC-3 cells in direct contact at a 1:1 ratio. After co-culture for 24 h, the cells were digested and the GFP + macrophages were sorted out by flow sorting. RNA extraction was performed using Invitrogen TRIzol (15,596,026,Thermo Scientific, USA).

cDNA is synthesized using reverse transcriptase with oligo(dT) primers (Vazyme). Real-time fluorescence quantitative PCR is performed on the CFX96 Real-Time PCR Detection System (Bio-Rad). The 25μL PCR reaction includes TBGreen™ Premix ExTaq™ II (Tli RNaseH Plus) (TaKaRa), 0.4 μM forward and reverse primer, and the RT product was diluted at least 10×. The primers of the genes were presented in supplementary Table S2.

Cytokine microarray

Cytokine and chemokine secretion from the co-culture system was assessed utilizing a semiquantitative Human Cytokine G-Series G5 Antibody Array and fluorescent detection (RayBiotech, #AAH-Cyt-G5, Inc., Norcross, GA), following the manufacturer's protocols. The glass chip containing the samples was thoroughly dried and subsequently scanned using the Cy3 channel (excitation

frequency = 532 nm) of the laser scanner Innopsys' InnoScan. After background signal subtraction and normalization to positive control signals, fluorescence intensity data from cell samples were analyzed by calculating the ratio of CAR THP-1 or hMDM-CAR cell signal to NC THP-1 or hMDM-Adv-mCherry cell signal.

In vivo murine pancreatic *cancer* model

Cell preparation involved adjusting the concentration of BxPC-3 luci + cells to 2×10^7 cells/ml. The cells were then mixed at a 1:1 ratio with Matrigel (354,234, Gibco, USA) and stored on ice temporarily. NOD/SCID mice (SPFBIOTECH, Beijing, China) aged 6–7 weeks were acclimatized under isolated conditions for one week and fasted for 6 h prior to surgery. Anesthesia was induced via intraperitoneal injection of 1% sodium pentobarbital (50 mg/kg), followed by depilation of the left lateral rib area with 10% sulfur sodium and disinfection using 75% alcohol. A 1.5 cm incision was made to expose the spleen and distal pancreas. Each mouse received an intrapancreatic injection of 50 µl of the aforementioned cell suspension, followed by layer-by-layer closure of the incision. Starting from the 5th day post-surgery, CAR THP-1,NC THP-1cells were injected intraperitoneally every 7 days, with each injection containing 1×10^7 cells in 500 µl of PBS. hMDM-Ad-mCherry, hMDM-CAR-c-MET were injected intraperitoneally every 7 days, with each injection containing 5×10^6 cells in 500 µl of PBS. Tumor burden was assessed every 7 days using bioluminescence imaging with IVIS Lumina III (PerkinElmer, USA) and quantified using Living Image® software. 35 days post-surgery, the remaining mice were euthanized. Daily monitoring of mouse survival and activity was conducted, and upon natural death or euthanasia, organs including the heart, lungs, liver, kidneys, gastrointestinal tract, and spleen, along with pancreatic tumors, were harvested, fixed in formalin, and subsequently embedded in paraffin for further experiments.

In vivo *biodistribution of CAR-M*

Pancreatic orthotopic tumor-bearing mouse models were established using BxPC-3 cells following the aforementioned protocol in NOD/SCID mice. Subsequently, healthy NOD/SCID mice and pancreatic orthotopic tumor-bearing NOD/SCID mice were each intraperitoneally injected with 1×10^7 NC THP-1 luci + or CAR THP-1 luci + cells. Bioluminescence imaging was performed at 0, 2, 4, 6, 12, and 24 h post-injection, followed by imaging every 24 h for a duration of 10 days. This longitudinal imaging approach allowed for the observation of the biodistribution of NC THP-1 luci + and CAR THP-1 luci + cells within the murine host over the experimental period.

In vivo *safety of CAR-M*

Intraperitoneal injections of 1×10^7 NC THP-1 luci + or CAR THP-1 luci + cells, as well as PBS as a control, were administered to NOD/SCID mice. One week post-injection, organs including the heart, lungs, liver, kidneys, spleen, and gastrointestinal tract, among others, were harvested for histological analysis following hematoxylin and eosin (H&E) staining to assess tissue damage. Additionally, serum samples were collected from mice to evaluate the biochemical safety profile of CAR THP-1 cells by assessing serum markers indicative of cardiac, hepatic, and renal function, among other serum parameters.

IF, H&E, and IHC staining

IF (immunofluorescence), H&E, and IHC staining were routinely performed as described. In brief, tissue sections were fixed and stained with corresponding primary antibody and incubated with Alexa Fluor 546-labeled secondary antibody (K1034G-AF594, Solarbio, China). The sections were photographed with an inverted fluorescence microscope (Olympus, Japan). The primary antibody used was human c-MET antibody (25,869–1-AP, Proteintech, China). Tissue sections were fixed and stained with DAB (SA-HRP), Tunel Cell Apoptosis Detection Kit (G1507, Servicebio, China).

In vitro *phagocytosis and cytotoxic assay of hMDM*

hMDM-CAR, hMDM-Adv-mCherry, hMDM-UTD cells were stained with CellTracker DeepRed (C34565, Thermo Fisher Scientific, MA, USA), and BxPC-3 cells were stained with CellTracker Green (C7025, Thermo Fisher Scientific, MA, USA). The stained cells were then co-cultured at a 3:1 E:T ratio. Flow cytometric analysis was performed on the co-culture system at 3, 6, 12, and 24 h post-co-culture. The hMDM cells were detected using the APC channel, while BxPC-3 cells were detected using the FITC channel. The percentage of FITC-positive cells within the APC-positive cell population was calculated as the phagocytic ratio of macrophages.

hMDM-CAR or hMDM-Adv-mCherry cells were co-cultured with BxPC-3 luci + cells at different E:T ratios. Bioluminescence signals from the co-culture systems were measured at 12, 24, and 48 h using IVIS Lumina III (PerkinElmer, USA) and quantified with Living Image® software to assess residual tumor cell abundance. The phagocytic efficiency of macrophages was evaluated by comparing the bioluminescence signals of target wells to those of control wells containing only tumor cells. Specifically, the phagocytic efficiency was calculated using the formula: Phagocytic efficiency = ((signal from the control well—signal from target well) / signal from the control

well) × 100%. This approach quantitatively measures the extent of tumor cell elimination by macrophages in the co-culture system.

In vivo *persistence of hMDM*

Pancreatic orthotopic tumor-bearing mouse models were established using BxPC-3 cells following the aforementioned protocol in NOD/SCID mice. hMDM-AdmCherry and hMDM-CAR-c-MET were stained with Dir cell membrane fluorescent dye probe (abs45153692, adsin, China). Each mouse was injected intraperitoneally with 5×10^6 cells. Imaging was performed with IVIS Lumina III (PerkinElmer, USA) at 3, 10, and 20d after injection.

Body weight and open field tests

Body weight and open field tests were performed 1 week after macrophage injection. All open-field testing occurred inside sound-insulated, ventilated multi-conditioning chambers (TSE Systems Ltd, Germany). The open-field arena (45 cm (l) × 45 cm (w) × 40 cm (h)) consisted of four transparent Plexiglas walls and a light gray PVC floor. Control animals for all experiments were tested under four equally spaced yellow lights (4 Lux across the floor of the open field) with 75–77 dB of white noise playing through the speakers of each box. An infrared light also illuminated the boxes so that an infrared camera could be used to record the tests. Animals were removed from their home cage by the tail and placed directly into the center of the open field. All open-field tests were 10 min in duration.

Statistical methods

Statistical analyses and graphical representations were performed using IBM SPSS Statistics 21.0 (SPSS Inc., Chicago, IL, USA) and GraphPad Prism 8.0 (La Jolla, CA, USA). Statistical analyses were performed to compare groups based on the distribution of data. Parametric Student's t-test or non-parametric Mann–Whitney U test was chosen for two-group comparisons.For comparisons involving three or more groups, one-way ANOVA or Kruskal–Wallis H test was utilized, followed by Dunnett-t or Tukey post hoc tests for pairwise comparisons as appropriate. Spearman or Pearson correlation analysis was used to assess linear correlations between variables according to different situations. Pearson's chi-square test evaluated correlations between categorical variables. Survival analysis was conducted using the Kaplan–Meier method and the Log-rank test, with optimal survival cut-off values determined by X-tile software. Statistical significance was set at $p < 0.05$ (two-tailed).

Results

c-MET is an ideal target for CAR-M

Bioinformatic analysis revealed a significant upregulation of c-MET in pancreatic cancer tissues compared to normal pancreatic tissues (Fig. 1A). Importantly, increased c-MET expression predicts shorter overall survival and progression-free survival in patients (Fig. 1B, C).

To validate these findings, tissue microarray analyses were conducted by using cancer tissue and peritumoral tissues from pancreatic cancer patients. Finally, 76 cases were enrolled for analysis. The proportion of strong and moderate staining in tumor tissues was significantly higher than in their paired peritumoral tissues (76.3% vs. 31.6%, $p < 0.0001$). Among the tumor tissues, 29 cases had a staining score greater than 8, compared to only one case in the peritumoral tissue. Interestingly, in all 76 cases, there was only one instance where the final staining score of the peritumoral tissue exceeded that of the tumor tissue. Additionally, 20 cases exhibited the same final staining score in both tumor and peritumoral tissues. However, in the remaining 55 cases, the final staining score in tumor tissues was higher than in peritumoral tissues (Fig. 1D, E, H-I).The optimal cutoff value for c-MET was determined to be 5 (0–5 vs. 6–12). Notably, a higher staining score predicted poorer survival after surgery (23 m (95%CI 18-43 m) vs not achieved,$p = 0.014$) (Fig. 1F). Further analysis involved examining the correlation between the expression of c-MET and various clinicopathological factors (age, sex, TNM staging, lymph node metastasis, differentiation grade, CEA, CA19-9, and CA125 levels). The results revealed that higher c-MET expression was associated with elevated levels of CA 19–9 ($r = 0.219$, $p < 0.029$) (Fig. 1G). Subsequent profiling of c-MET expression across pancreatic cancer

(See figure on next page.)

Fig. 1 **A** Bioinformatic analysis showed the different expression levels of c-MET in pancreatic cancer tissues compared to normal pancreatic tissues. **B** Bioinformatic analysis showed correlations between c-MET expression and overall survival in pancreatic cancer patients. **C** Bioinformatic analysis showed correlation between c-MET expression and progression-free survival in pancreatic cancer patients. **D** Representative IHC staining of c-MET expression in tumor tissue and peritumoral tissues. **E** Representative IHC staining of different levels of c-MET expression in tumor tissue. **F** Higher IHC score of c-MET predicted poorer overall survival of patients after surgery. **G** Spearman analysis showed a positive correlation between CA19-9 and c-MET. **H** the details of the IHC score of c-MET in all 76 cases of tumor tissue and its paired peritumoral tissue. **I** A paired t-test was used to test the c-MET IHC scores of tumor and peritumoral tissue. **J** FCM results showed that the BxPC-3 cell line had the highest expression of c-MET (***, $p < 0.001$;****, $p < 0.0001$)

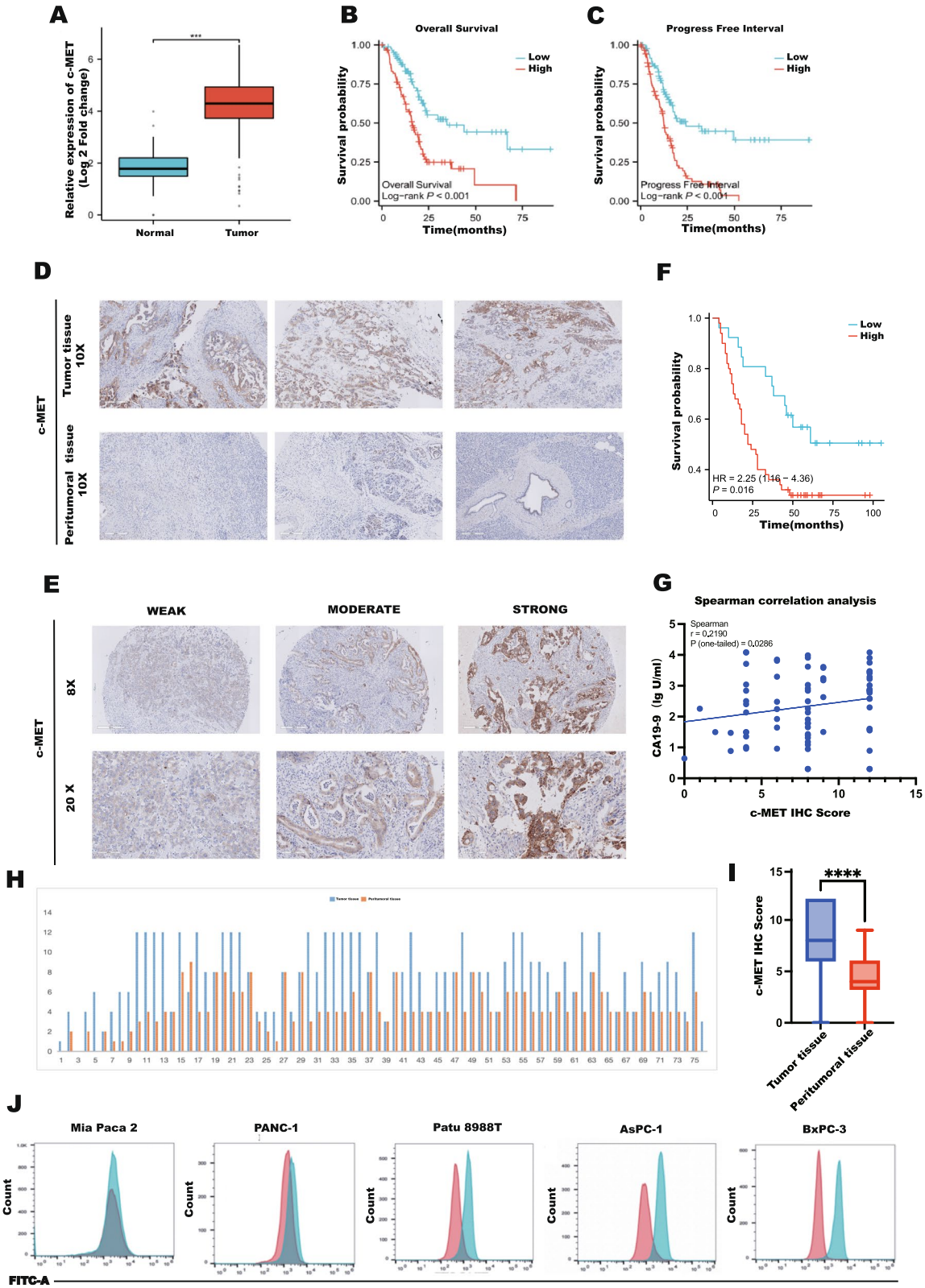

Fig. 1 (See legend on previous page.)

cell lines revealed widespread expression in most cell lines. Notably, the BxPC-3 cell line exhibited the highest expression level, warranting its selection as the target cell line for subsequent experiments (Fig. 1J). CAR-M-c-MET has high affinity and specific killing capacity to c-MET expressing pancreatic cancer cells

Following successful sequence construction and plasmid synthesis, lentiviral vectors were utilized for packaging, and the immortalized human monocyte line THP-1 was used to establish stably passaged CAR-M-c-MET THP1 cells. Upon transfection, THP-1 cells were induced to adhere and differentiate into M0 macrophages using PMA, followed by polarization into pro-inflammatory phenotype using LPS and IFN-γ (Fig. 2A). Subsequently, the GFP sequence was fused with the CAR sequence via the T2A sequence, enabling the isolation of THP-1 cells stably expressing GFP (CAR+) through flow sorting. These CAR THP-1 cells were then expanded and cultured in vitro for subsequent experiments (Fig. 2B). Control THP-1 cells expressing GFP alone were also generated.

To validate c-MET targeting efficacy, both CAR THP-1 and control pro-inflammatory polarized THP-1 cells were incubated with recombinant his tag-Hu c-MET protein, followed by FCM analysis using an anti-His tag antibody. The results demonstrated robust binding of CAR THP-1 cells to the c-MET target (Fig. 2C). Further functional assessments involved co-culturing pro-inflammatory polarized CAR+THP-1 and pro-inflammatory control THP-1 cells with mCherry-labeled BxPC-3 pancreatic cancer cells at an E:T ratio of 5:1. FCM analyses conducted at various time points revealed significantly higher phagocytic binding efficiency of CAR THP-1 cells compared to control THP-1 cells. Notably, peak phagocytosis efficiency was observed at 2–4 h, reaching up to 20%, albeit showing a slight decline at 6 h while still maintaining approximately fivefold higher efficiency than control THP-1 cells (Fig. 2D).

Subsequent investigations involved co-culture experiments at E:T ratios of 10:1 and 5:1 for 24 h to assess residual tumor cell presence. Remarkably, CAR THP-1 cells exhibited significantly reduced residual tumor cells compared to control THP-1 cells (Figs. 2E-F).

To demonstrate that the effect of CAR THP-1 cells is derived from the efficacy of intracellular activation signal domains. The intracellular domain(ICD)-depleted CAR sequence was constructed and transfected into THP-1 cells. We used it as another control group and repeated the above experiments. We found that CAR^{-ICD} THP-1 had a significant reduction in the phagocytic ability to tumor cells (Supplement Fig. 1A).

Additionally, BxPC-3 cells transfected with Luciferase were employed to evaluate killing efficiency via bioluminescence assays at different E:T ratios and co-incubation times. The superior killing capacity of CAR THP-1 cells over control THP-1 cells was observed with dose and time-dependent responses (Fig. 3A, B). In addition, in order to prove that CAR THP-1 has stronger killing ability than NC THP-1 without inducing PRO-INFLAMMATORY phenotype, BxPC-3 cell line was co-cultured without inducing pro-inflammatory phenotype, and the killing ability of CAR THP-1 was closely related to its intracellular activation signal domain (Supplement Fig. 1B).

The above experiments were also repeated in mouse BMDM cell lines. We found that BMDM-CAR-c-MET could bind to phagocytoma and kill BxPC-3 cells effectively (Supplement Fig. 1C, D).

Moreover, quantification of lactate dehydrogenase (LDH) in the co-culture supernatant revealed markedly elevated levels in the CAR+THP-1 group compared to the control THP-1 group, indicating enhanced tumor-cell killing activity (Fig. 3C). Finally, confocal microscopy observations confirmed increased phagocytic events by CAR+THP-1 cells on tumor cells, further validating their potent anti-tumor activity (Fig. 3D).

Moreover, live cell high-speed laser confocal real-time imaging system demonstrated that CAR THP-1 could also kill the surrounding tumor cells by releasing cytotoxic cytokines and trogocytosis (Supplement video 1). However, the killing effect of NC THP-1 on tumor cells was not observed (Supplement video 2).

The results demonstrated that this novel CAR-M-c-MET could effectively bind to and kill c-MET-overexpressing pancreatic cancer cell lines.

CAR-M-c-MET improves cytotoxic chemotherapeutic efficacy in pancreatic cancer cells

To explore potential synergistic effects, we investigated the combination of CAR-M therapy with various chemotherapeutic drugs. Initially, BxPC-3 luci+cells were

(See figure on next page.)

Fig. 2 **A** Schematic diagram of the CAR structure and CAR THP-1 construction, induction, phagocytosis, and killing effect. **B** Purification of CAR THP-1 by FCM sorting. **C** FCM showed that CAR THP-1 could effectively bind His-tag hu-c-MET recombinant protein. **D** CAR THP-1 or NC THP-1 was co-cultured with BxPC-3 mcherry+at a ratio of 5:1, and the co-culture system was detected by FCM at 30 min, 2 h, 4 h, and 6 h. **E** CAR THP-1 or NC THP-1 was co-cultured with BxPC-3 mcherry+at a ratio of 10:1 for 24 h, and residual BxPC-3 mcherry+cells were detected by FCM. **F** CAR THP-1 or NC THP-1 was co-cultured with BxPC-3 mcherry+at a ratio of 5:1 for 24 h; residual BxPC-3 mcherry+cells were detected by FCM

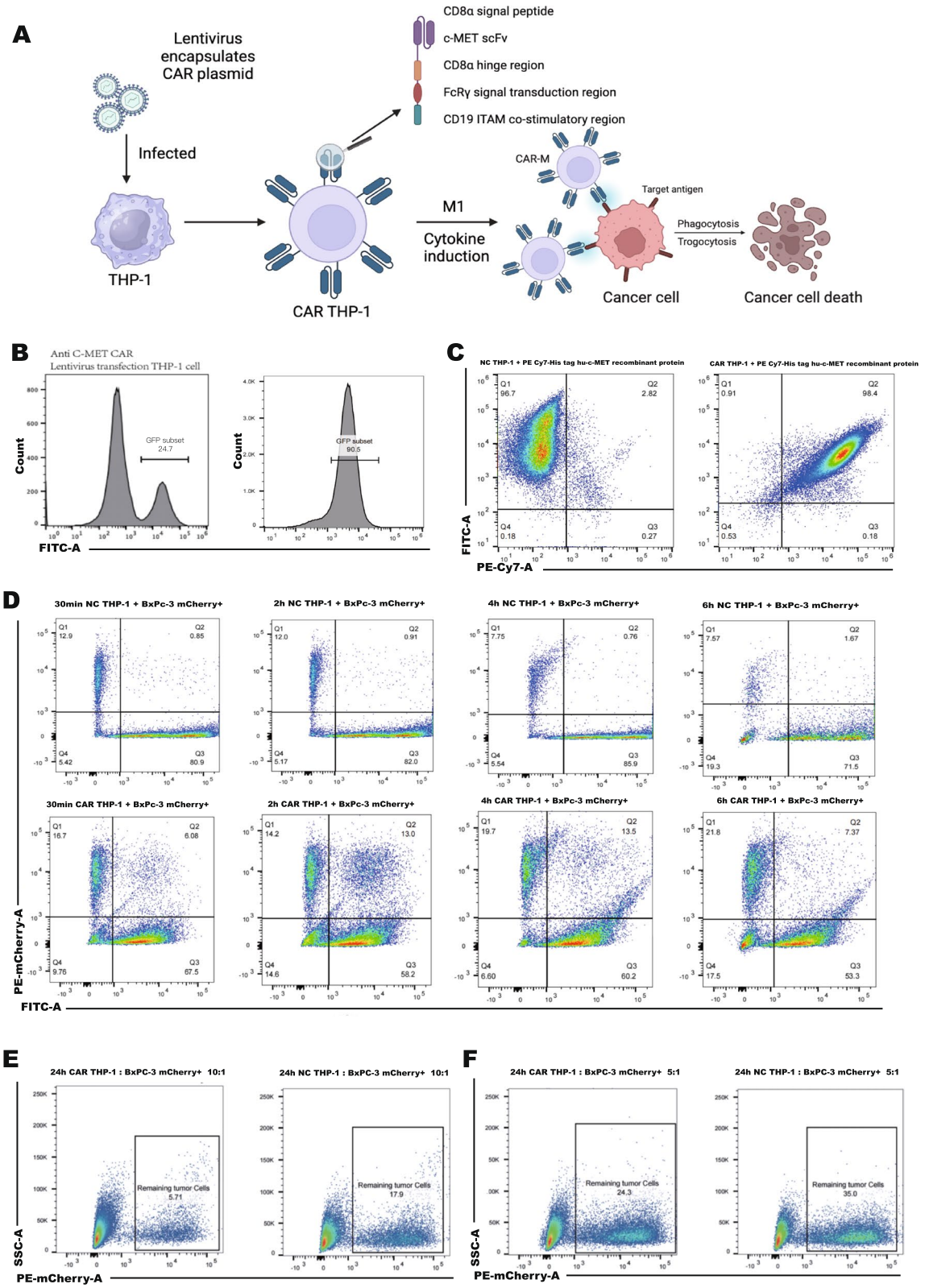

Fig. 2 (See legend on previous page.)

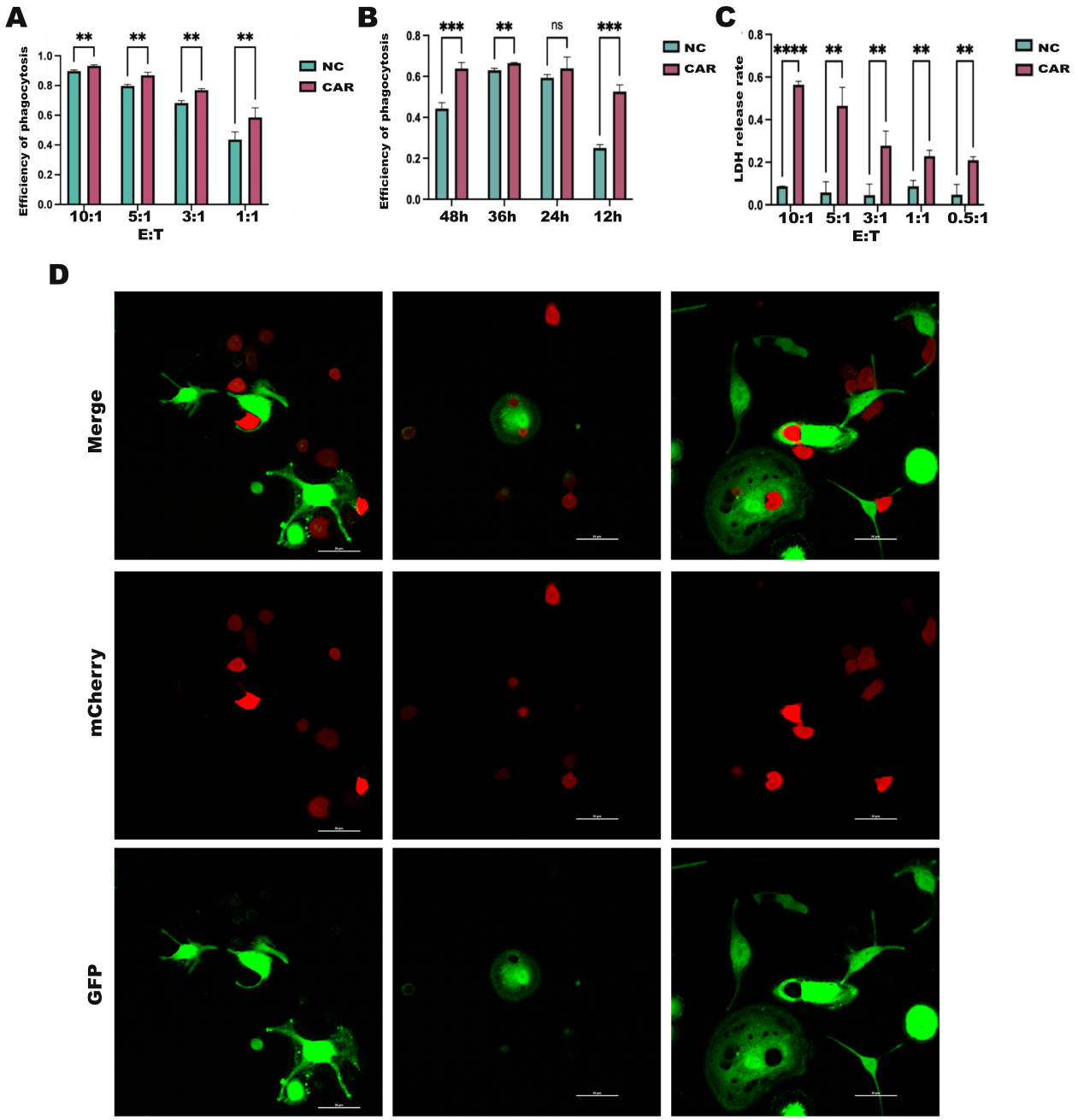

Fig. 3 **A** CAR THP-1 or NC THP-1 and BxPC-3 luci + cells were co-cultured for 24 h at different E: T ratios and bioluminescence imaging was performed in the co-culture system. **B** CAR THP-1 or NC THP-1 and BxPC-3 luci + cells were co-cultured at 5:1 for different times, and bioluminescence imaging was performed in the co-culture system. **C** CAR THP-1 or NC THP-1 and BxPC-3 were co-cultured for 24 h at different E: T ratios, and LDH content in the supernatant of the co-culture system was detected. **D** The co-culture system was photographed by fluorescence confocal microscope, and the process of macrophages extending pseudopodia, endocytosis, and lysis of BxPC-3 cells.(**, $p < 0.01$;***, $p < 0.001$)

incubated with drugs for 24 h. Following drug removal, CAR-THP-1 cells were introduced and co-incubated for an additional 24 h (Fig. 4A). Evaluation of residual BxPC-3 cells through bioluminescence signal detection revealed comparable efficacy between CAR-THP-1 monotherapy and cytotoxic chemotherapeutic drugs alone. Strikingly, simultaneous administration of cytotoxic chemotherapeutic drugs and CAR-THP-1 resulted in a significant reduction in residual tumor cells (Fig. 4B). Concurrently, quantification of LDH

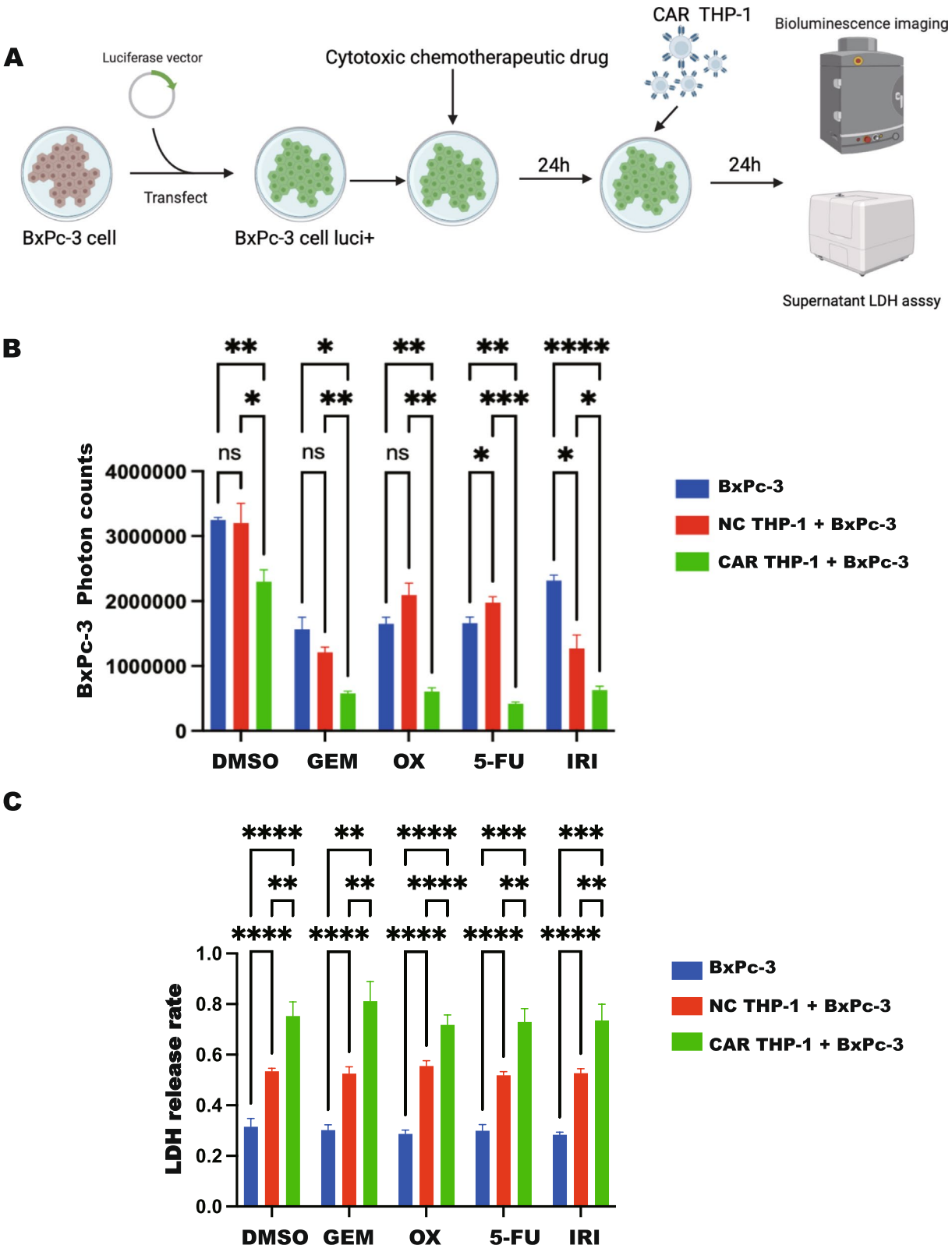

Fig. 4 **A** Schematic diagram of the flow of CAR THP-1 combined with cytotoxic chemotherapy drugs to intervene in BxPC-3 luci + cells. **B** BxPC-3 luci + cells were treated with CAR THP-1 or NC THP-1 combined with different cytotoxic chemotherapy drugs, and the residual BxPC-3 luci + cells were detected by bioluminescence imaging. **C** LDH content test in the supernatant of the treatment systems (*, $p < 0.05$;**, $p < 0.01$;***, $p < 0.001$;****, $p < 0.0001$)

levels in the co-culture supernatant corroborated these observations, further supporting enhanced tumor cell killing with combination therapy (Fig. 4C).

CAR-M-c-MET shows an activated immune state after co-culture with pancreatic cancer cells

To elucidate the mechanism underlying CAR-M-mediated tumor cell killing and the phenotypic changes of CAR-M cells, transcriptome sequencing of sorted macrophages from the co-culture system was employed and cytokine microarray analysis on co-culture supernatants was also carried out (Fig. 5A). To thoroughly explore the spontaneous phenotypic or functional changes of CAR-M, neither IFN-γ or LPS was added into the medium to induce CAR-M or control macrophages. Notably, CAR THP-1 exhibited elevated secretion of GM-CSF and reduced secretion of interleukin-10 (IL-10) compared to NC THP-1 (Fig. 5B, C). This suggests that CAR THP-1 cells gradually change towards a pro-inflammatory phenotype upon encountering tumor cell surface antigens in the co-culture system. In contrast, NC THP-1 cells lack such activation signals and tend towards an anti-inflammatory phenotype.

Cluster analysis showed that CAR THP-1 and NC THP-1 showed significant differences at the transcriptome level (Fig. 5D-E). Transcriptome analysis further delineated significant differences between CAR THP-1 and NC THP-1, with differentially expressed genes primarily enriched in intracellular signal transduction, gene transcription, and immune signaling pathways. Enriched cellular components included immune synapse formation and cell membrane transport, underscoring the involvement of these processes in CAR-M-mediated tumor cell killing (Fig. 5F-I). The details of the differentially expressed genes are presented in Table S3.

In addition, some classic markers or cytokines of pro- or anti-inflammatory phenotypes were validated by qPCR in CAR THP-1 and NC THP-1 with or without co-culture with BxPC-3 cell line. We found CAR THP-1 was more biased towards a pro-inflammatory phenotype after co-culture with tumor cells. (Fig. 5J-K).

CAR-M-c-MET inhibits tumor progression in a pancreatic cancer murine model

To further validate the efficacy of CAR-M therapy, an orthotopic pancreatic tumor-bearing model using BxPC-3 luci + cells in immunodeficient mice was established. Five days post-surgery, CAR THP-1 cells were intraperitoneally administered once weekly, and tumor burden was monitored weekly using a small animal imaging device (Fig. 6A). The results revealed an extension in survival time of mice treated with CAR-THP-1 cells compared to the control group (Fig. 6B), accompanied by a significant reduction in tumor burden (Fig. 6C). Consistent findings were obtained through quantitative analysis of tumor burden using bioluminescence imaging (Fig. 6D).

By HE staining of the sections of the specific organs of the mice, it was found that there were many micrometastases distributed in the liver of the PBS and NC THP-1 mice but not in the liver of the CAR THP-1 mice (Fig. 6E). Pancreatic tumors of the CAR THP-1 group showed larger necrotic areas by HE staining and TUNEL staining (Fig. 6F). There is no evidence of organ damage in vital organs, including the lungs, stomach, and intestine (Fig. 6G). Serum markers for liver and kidney function, myocardial enzymes, pancreatic function, inflammatory proteins, calcium, and phosphorus metabolism demonstrated that CAR THP-1 had no significant effect on the function of vital organs in mice and was reliable in safety (Supplement Fig. 2 and Fig. 3). The safety of CAR THP-1 was also confirmed by body weight and open field tests (Supplement Fig. 4).

Further, following intraperitoneal injection, CAR THP-1 showed specific intratumoral migration capacities compared to the NC THP-1 (Fig. 6H-I).

Construction and validation of CAR-M-c-MET-hMDM

Considering the potential risks associated with the use of immortalized tumor cell lines and lentiviral vectors in clinical translational research, a strategy utilizing human PBMCs to derive primary macrophages in vitro through cytokine induction was employed. Subsequently, adenovirus vectors to transfect these macrophages with the aforementioned CAR sequences were employed, thereby generating human monocyte-derived CAR-M (CAR-M-hMDM). Overcoming the

(See figure on next page.)

Fig. 5 **A** Co-culture of BxPC-3 cells with CAR THP-1 or NC THP-1, macrophages were sorted out by FCM and subjected to RNA-seq, and the co-culture supernatant was detected by cytokine microarray. **B** Quantitative detection and T-test of GM-CSF in co-culture supernatant. **C** Quantitative detection and T-test of IL-10 in co-culture supernatant. **D** Volcano map of differentially expressed genes by RNA-seq of CAR THP-1/NC THP-1. **E** Heat map of CAR THP-1/NC THP-1 RNA-seq. **F-I** GO and KEGG enrichment of differentially expressed genes. (J-K) CAR THP-1 and NC THP-1 coculture with or without BxPC-3 were sorted for qPCR (**, $p < 0.01$;***, $p < 0.001$)

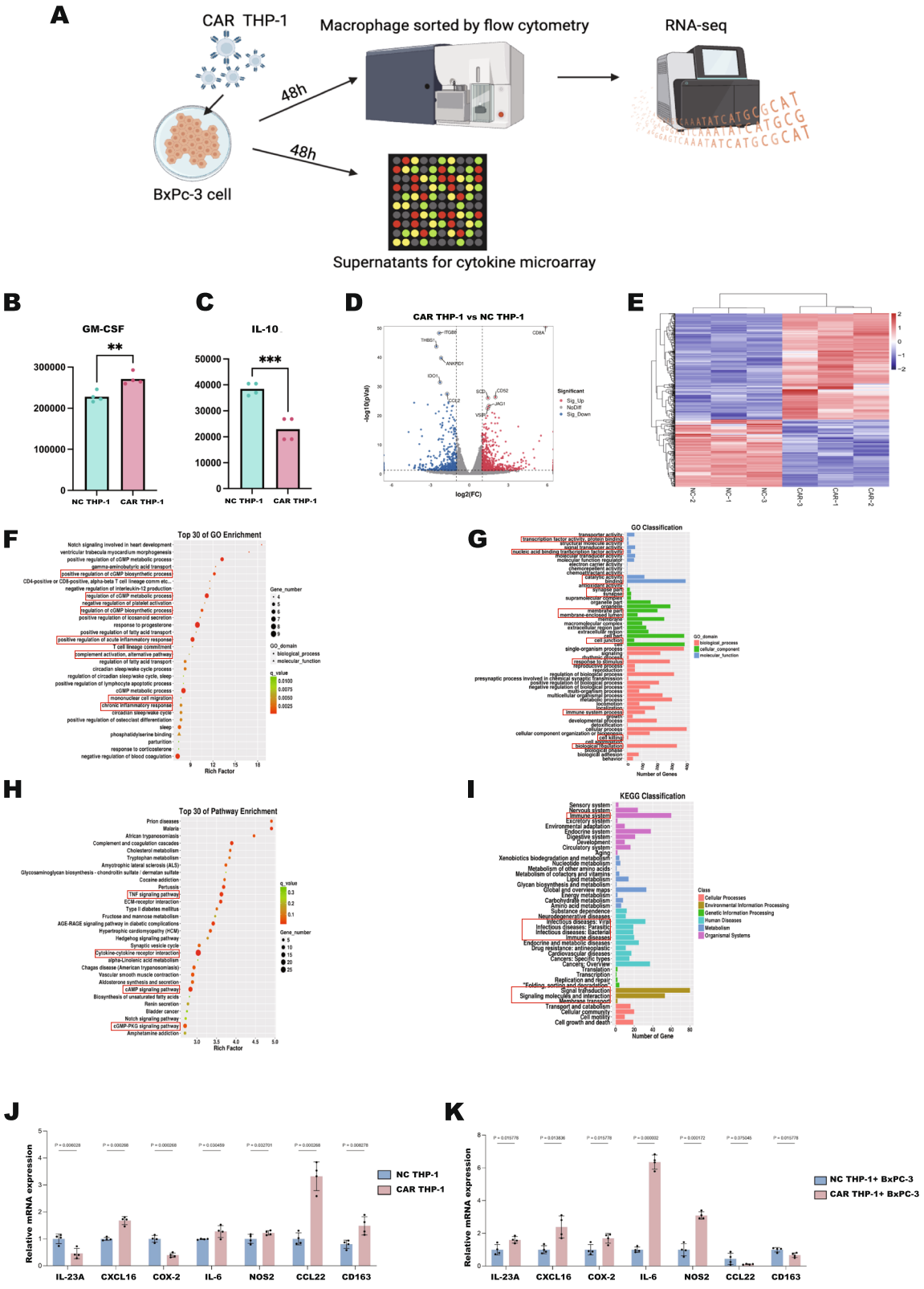

Fig. 5 (See legend on previous page.)

challenge of macrophage transfection, high transfection efficiency at an optimal multiplicity of infection (MOI) of 3000 was achieved (Figs. 7A-7D).

Furthermore, upon co-culture with BxPC-3 cells, CAR-M-c-MET-hMDM exhibited significantly enhanced phagocytosis efficiency compared to untreated macrophages (UTD) and macrophages transfected with empty adenovirus vectors at 3 h, 6 h, and 12 h (Fig. 7E-G). This finding was further corroborated through bioluminescence detection, where the CAR-M group displayed markedly superior phagocytosis efficiency compared to the control adenovirus group at 12 h, 24 h, and 48 h post-co-culture, with the disparity progressively widening over time (Fig. 7H-J). The results compared with UTD macrophage can be found in Supplement Fig. 1E. Subsequently, we constructed CAR-M-CD3ζ with CD3ζ as the intracellular domain and harvested the same results during co-culture with BxPC-3 cells in vitro (Supplement Fig. 5A-G).

The CAR-M-c-MET-hMDM cells showed an active immune state, consistent with the RNA-sequencing and cytokine array results obtained from the CAR-M-c-MET-THP1 cells (Fig. 7K-N, Supplement Fig. 5H-N). The details of the differentially expressed genes are presented in Tables S4 and S5.

At the same time, to clarify the correlation between the killing effect of CAR-M on tumor cells and the expression of c-MET target and the role of CAR-M in different Kras mutation types. We repeated the above experiments in three pancreatic cancer cell lines with different target expression levels and different Kras mutation types. We found that CAR-M had an effect on cell lines with different Kras mutation types, and the magnitude of the effect was related to the amount of c-MET target expression (Fig. 8A, B).

In addition, we constructed hMDM-CAR-HER2-CD3ζ and co-cultured it with BxPC-3 cells. We found that hMDM-CAR-HER2-CD3ζ did not efficiently kill BxPC-3 cells. It was also verified again that the killing effect of CAR-M on tumor cells was dependent on the binding of CAR to its target to initiate activation signals (Fig. 8C, D).

Subsequently, we also verified it in an orthotopic pancreatic tumor-bearing model using BxPC-3 luci + cells in immunodeficient mice. For the effect of CAR-c-MET-hMDM in vivo, we found that CAR-c-MET-hMDM could effectively reduce the tumor burden in mice (Fig. 8E). Meanwhile, we stained CAR-c-MET-hMDM and hMDM-Adv cells with Dir signal and continuously imaged them to observe the persistence of macrophages in vivo. Intraperitoneal injection macrophages could maintain activity in mice for more than 20 days (Fig. 8F). Finally, CAR-c-MET-hMDM could significantly prolong the survival time of mice (Fig. 8G).

Discussion

Although several clinical trials of CAR-T cells targeting Claudin18.2, HER2, EGFR, and Mesothelin have shown potential efficacy in inhibiting the progression of pancreatic cancer, CAR-T cells have significant challenges in treating this disease [19–21]. These challenges include limited T cell penetration into the tumor microenvironment, lack of co-stimulating signals, and intense immunosuppression within pancreatic tumors [7]. Transfusing autologous macrophages, which are expanded and activated in vitro, has been explored in clinical trials for solid tumors. The safety and feasibility of transfusing up to 3×10^9 autologous PBMC-derived macrophages have been demonstrated, but unfortunately, no notable antitumor effects were observed [22–24].

CAR-M cells offer several advantages, specifically for pancreatic cancer. Macrophages exhibit formidable infiltration capabilities into pancreatic cancer tissues. By adding chimeric antigen receptors (CARs), CAR-M cells possess specific and non-specific killing capacities. Additionally, CAR-M cells may play a role in inducing an immune-activated tumor microenvironment. Importantly, CAR-M cells carry a lower risk of GVHD [14, 25]. While CAR-M cell therapy in solid tumors and degenerative diseases has gained increasing attention [25, 26], its effects on pancreatic cancer remain unexplored.

c-MET is an oncogene that exhibits increased expression across several solid tumors and, therefore, is thought to play a crucial role in tumor progression. Clinical trials using antibodies or inhibitors against c-MET did

(See figure on next page.)

Fig. 6 **A** Flow chart of establishment of orthotopic pancreatic transplantation tumor model in NOD/SCID mice and verification of anti-tumor effect of CAR THP-1 i.p. **B** Survival curves of orthotopic pancreatic transplantation tumor model. **C** Bioluminescence image of orthotopic pancreatic transplantation tumor model. **D** Quantitative analysis and t-test of tumor burden on the last bioluminescence images of orthotopic pancreatic transplantation tumor model. **E** HE staining of tumor tissue. **F** TUNEL detection of tumor tissues. **G** HE staining of liver (micrometastasis), lung, stomach, intestine, kidney and heart. (H) CAR THP-1 luci + or NC THP-1 luci + cells were intraperitoneally injected into orthotopically tumor-bearing mice and healthy mice, and the biodistribution of THP-1 cells was detected by bioluminescence. **I** CAR THP-1 luci + /NC THP-1 luci + cells were intraperitoneally injected into orthotopically tumor-bearing mice and healthy mice for 5 days, and the distribution of THP-1 cells in various vital organs of mice was detected by bioluminescence (*, $p < 0.05$)

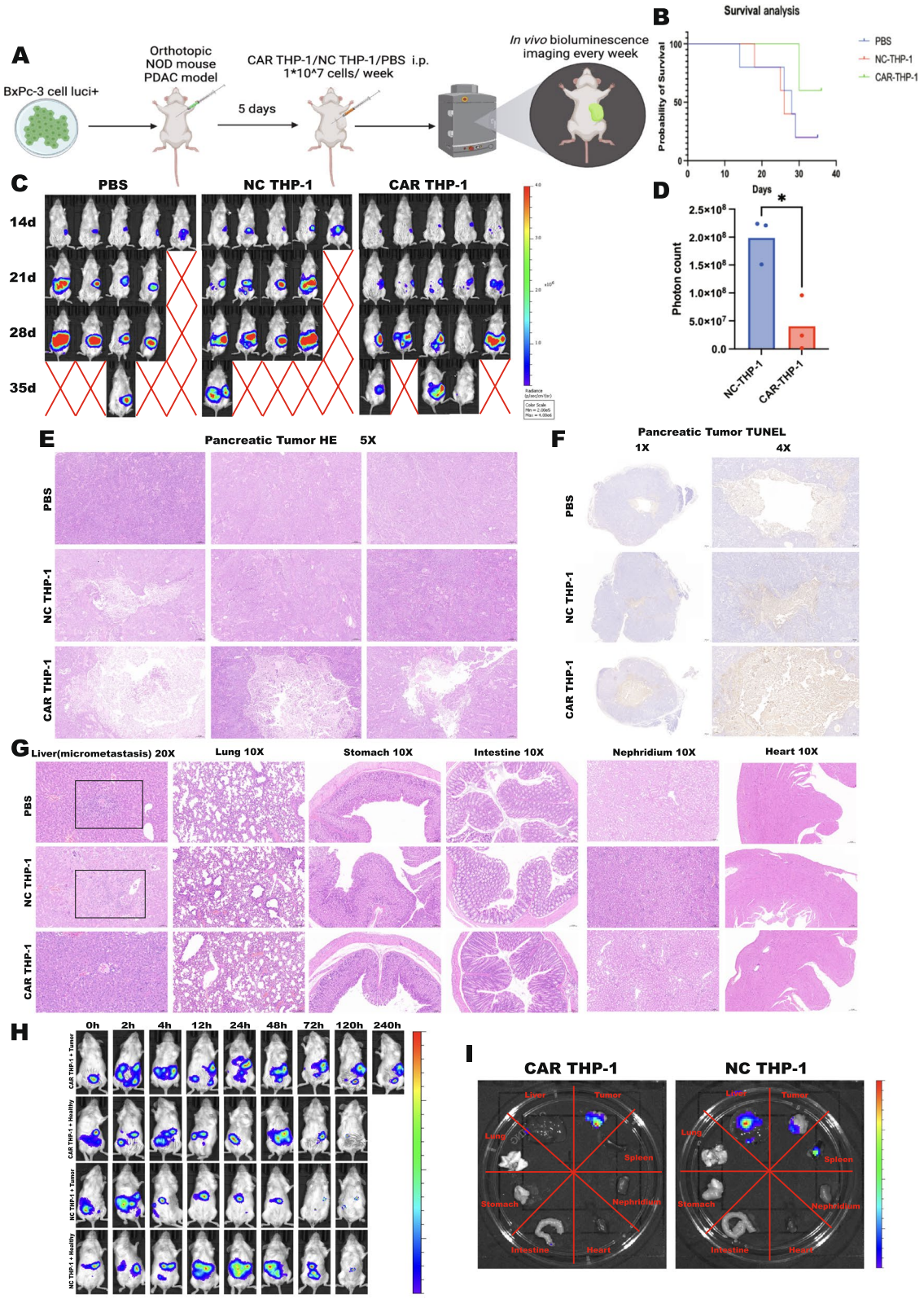

Fig. 6 (See legend on previous page.)

not result in severe side effects among cancer patients [27–30]. In this study, bioinformatic and tissue microarray analysis consistently revealed significantly elevated c-MET levels in tumor tissues compared to adjacent peritumoral tissues. Increased levels of c-MET expression correlated with poorer patient survival. Therefore, c-MET was chosen as target for constructing CAR-M cells.

Several intracellular activation domains of CAR-M have been reported; however, the results were inconsistent in activation capacity [7]. Therefore, we tested the FCRγ signaling transduction region, the CD19 ITAM co-stimulatory region, and the CD3ζ signaling transduction region. Firstly, we generated CAR-M-c-MET THP1 cells by infecting THP1 cells with a lentivirus vector, resulting in stable CAR expression. This approach allows for the rapid production of a large number of CAR-M-c-MET cells for both in vitro and in vivo animal studies. The intracellular activation domain of CAR-M-c-MET THP1 cells comprises the FCRγ signaling transduction region and the CD19 ITAM co-stimulatory region. In vitro experiments, these CAR-M-c-MET THP1 cells exhibited high affinity for c-MET-expressing human pancreatic cancer cells.It has been reported that CAR-M shows more killing activity after pro-inflammatory induction [31]. To further assess their killing capacity, we induced control THP1 cells into a pro-inflammatory polarized state using IFN-γ and LPS. Compared to the control pro-inflammatory polarized THP1 cells, the CAR-M-c-MET THP1 cells demonstrated significantly more vigorous killing activity and phagocytosis. Remarkably, CAR-M-c-MET THP1 cells could rapidly infiltrate tumor tissues and persist for over ten days. In a murine pancreatic cancer model, intraperitoneal transfusion of these cells substantially reduced the tumor burden.

Cytotoxic chemotherapy is the mainstay therapy for pancreatic cancer in palliative, adjuvant, and neoadjuvant settings [5, 32, 33]. Therefore, in this study, we also tested the potential synergistic role of common chemotherapeutic agents. The results demonstrate that CAR-M cells can enhance the effects of most of the cytotoxic agents. These findings provide a compelling rationale for exploring CAR-M alongside standard chemotherapy regimens in patients, potentially offering a synergistic approach to improve treatment outcomes in advanced pancreatic cancer. Such synergistic interactions between CAR-M therapy and chemotherapy hold promise for enhancing therapeutic efficacy and warrant further investigation in clinical settings. However, it is essential to note that lentivirus-infected CAR-M-c-MET THP1 cells are unsuitable for clinical trials due to their oncogenic potential in vivo.

Primary macrophages often stand as stalwart guardians against viral invaders. However, their natural resistance to viral vectors poses a significant challenge in generating sufficient CAR-M cells for pre-clinical experiments and clinical trials. Herein, we constructed a novel adenovirus-modified vector explicitly designed for delivering CARs. This vector exhibits remarkable transfection efficiency. Moreover, it can lock the CAR-M cells in an immune-activated state, enhancing their potency and effectiveness. Furthermore, CAR-M-c-MET-hMDM cells were successfully constructed using the adenovirus vectors produced through the in-house GMP(Good Manufacturing Practice) production line. These cells hold promise for potential use in clinical trials. Notably, we observed similar findings in CAR-M-c-MET-THP1 cells replicated in CAR-M-c-MET-hMDM cells. As a result, the efficacy of CAR-M-c-MET in treating pancreatic cancer has been validated.

Two primary concerns regarding CAR-M-c-MET cells are safety and anti-inflammatory polarization. After the transfusion of CAR-M-c-MET cells, serum markers for vital organ functions and pathological analyses revealed no severe systematic side effects, thus confirming its safety. To prevent anti-inflammatory polarization during interactions with pancreatic cancer cells and to enhance killing and phagocytosis ability, we employed LPS and IFN-γ to induce pro-inflammatory polarization in CAR-M-c-MET-THP1 cells. Additionally, CAR-M-c-MET-hMDM cells spontaneously remained in a pro-inflammatory state after adenovirus-vector-CAR transfection. Notably, CAR-M-c-MET-THP1 cells and CAR-M-c-MET-hMDM cells without pro-inflammatory induction also exhibited an immune-activated state, with no elevation of anti-inflammatory markers, as evidenced by cytokine array and mRNA sequencing results.

(See figure on next page.)

Fig. 7 **A**-**C** FCM analysis of the G4S tag of CAR-M-hMDM represents transfection efficiency. **D** The positive rate of hMDM mcherry + under different MOI transfection conditions was photographed by fluorescence microscope. **E-G** FCMdetected the proportion of double positive macrophages in the co-culture system after 3,6,12 h of CAR-M-hMDM and control macrophages co-cultured with BxPC-3 cells. **H-J** Residual tumor cells in the co-culture system was detected by bioluminescence after CAR-M-hMDM and control macrophages co-cultured with BxPC-3 luci + cells for 12,24,48 h, and the phagocytosis efficiency was calculated. **K**, **L** After co-cultured with BxPC-3 cells, RNA-seq was performed on macrophages. GO and KEGG enrichment of differentially expressed genes. **M**, **N** Quantitative detection and T test of GM-CSF and IL-10 in CAR-M-hMDM, hMDM-UTD and hMDM-Ad-mCherry co-culture supernatant (*, $p < 0.05$; **, $p < 0.01$;***, $p < 0.001$)

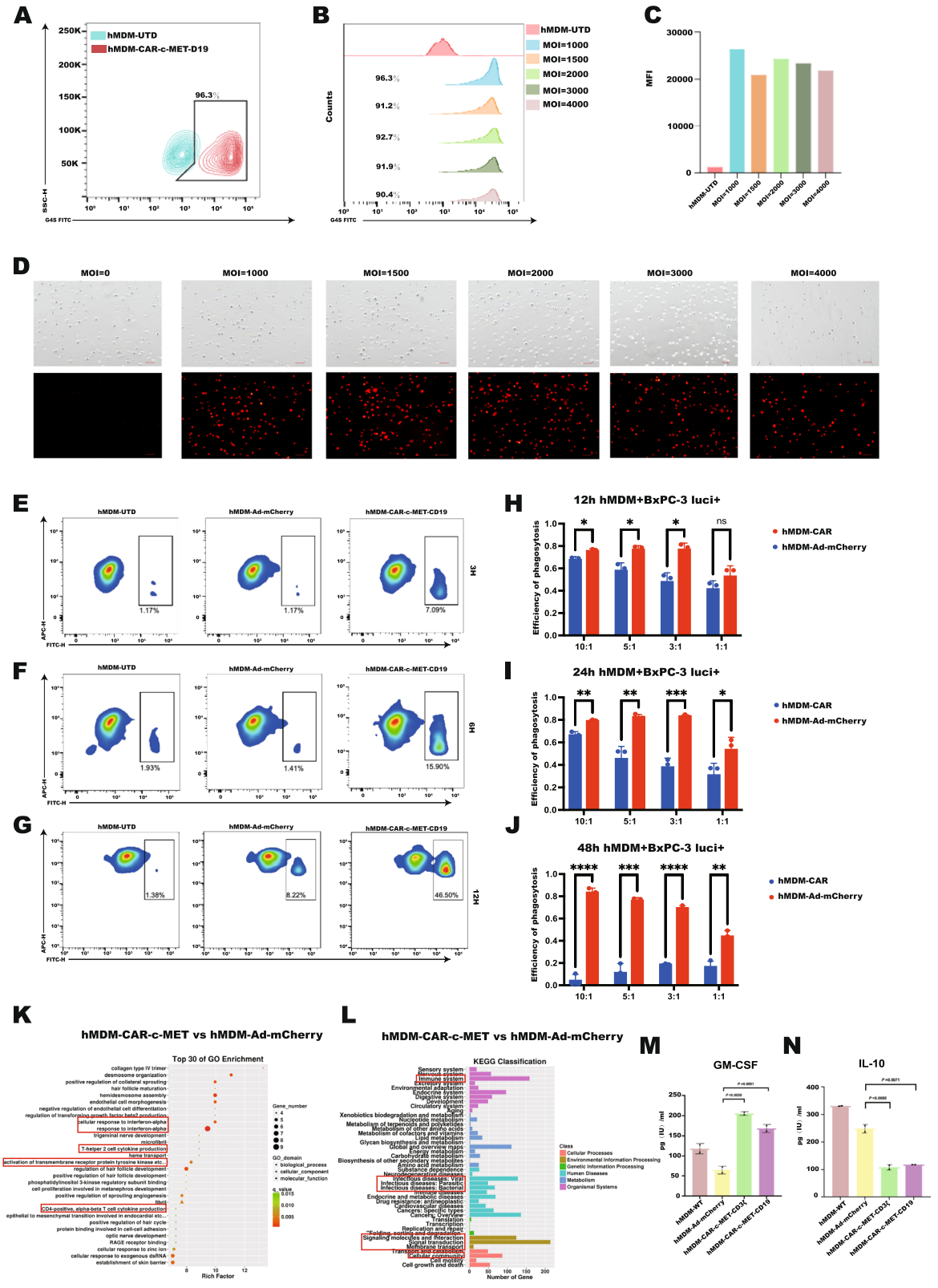

Fig. 7 (See legend on previous page.)

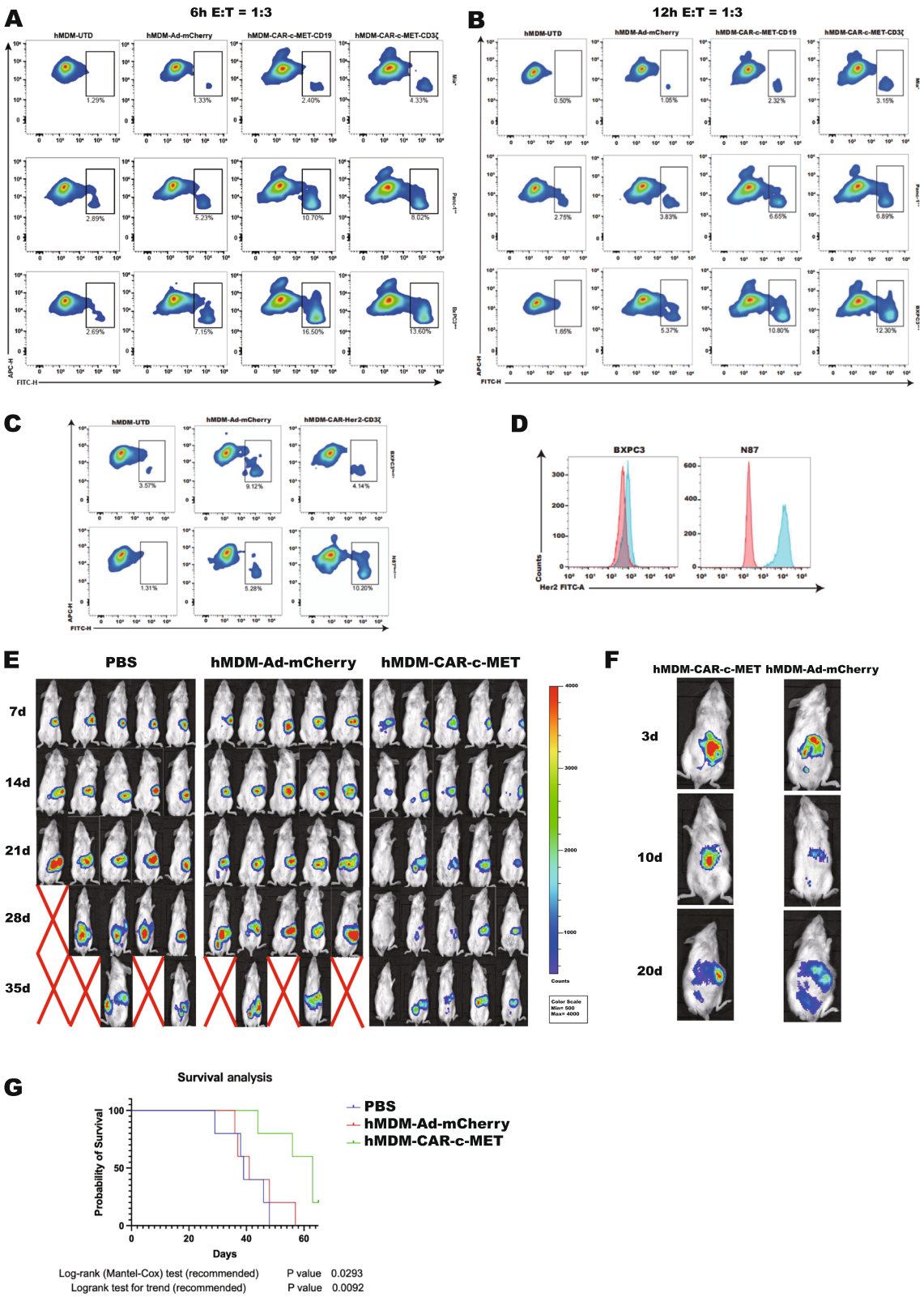

Fig. 8 **A**, **B** hMDM-UTD,hMDM-Adv,hMDM-CAR coculture with BxPC-3, Mia Paca 2,PANC-1 cell for 6 h or 12 h at a ratio of 1:3. **C** hMDM-UTD,hMDM-Adv and hMDM-CAR-HER2 coculture with BxPC-3 and N87 for 12 h at a ratio of 1:3. **D** BxPC-3, N87 HER2 expression detection. **E** the dynamic tumor burden after different treatments. **F** the biodistribution of hMDM-CAR after i.p. **G** CAR-c-MET-hMDM could prolong the survival of the orthotopic tumor bearing mice

Limitations

While the study concentrates on the therapeutic potential of this approach in pancreatic cancer, it is imperative to acknowledge the overarching challenges that solid tumors generally encounter with CAR-based treatments. The stroma barrier of solid tumors, which includes the extracellular matrix and tumor-associated fibroblasts, may restrict the infiltration and distribution of CAR-M cells [34, 35]. Additionally, macrophages within the tumor microenvironment may undergo reprogramming into anti-inflammatory phenotypes that foster tumor growth, potentially diminishing the anti-tumor capabilities of CAR-M cells [36, 37]. The heterogeneity of solid tumors also presents challenges for target selection, which could impact the effectiveness of CAR-M therapy [38]. Despite the promising results of CAR-M cells in vitro, their actual impact on solid tumor treatment remains to be confirmed through further clinical studies. The road to effective treatment for solid tumors is still long and fraught with difficulties. However, our research on CAR-M in pancreatic tumors represents a step forward in exploring potential solutions for this complex problem.

Conclusion

This study comprehensively demonstrated the safety and efficacy of CAR-M-c-MET therapy in treating pancreatic cancer in vitro and in vivo models. The CAR-M-c-MET cells have formidable capacities to suppress pancreatic cancer progression and enhance the effectiveness of cytotoxic chemotherapy. No discernible side effects were observed in murine models. Clinical trials to further validate its safety and efficacy in patients with pancreatic cancer are of great clinical significance.

Supplementary Information

The online version contains supplementary material available at https://doi.org/10.1186/s12943-024-02184-8.

Supplementary Material 1.
Supplementary Material 2.
Supplementary Material 3.
Supplementary Material 4.
Supplementary Material 5.
Supplementary Material 6.
Supplementary Material 7.

Acknowledgements

We extend our gratitude to Prof. Wenming Wu from the Department of General Surgery, Peking Union Medical College Hospital, for his help in organizing this study. Additionally, we appreciate the support provided by Laboratory Animal Research Facility and Biomedical Engineering Facility of National Infrastructures for Translational Medicine, Institute of Clinical Medicine, Peking Union Medical College Hospital, Chinese Academy of Medical Sciences and Peking Union Medical College and the Central Lab of the Basic Research Institution of the Chinese Academy of Medical Sciences. Special thanks go to the generous peripheral blood donors, whose contributions have been instrumental in our research endeavors. We thank Prof.Huanwen Wu from Department of Pathology , Peking Union Medical Colleg Hospital, for this great patholgoical work. We thank Ms.Yan Cao from Department of General Surgery, Peking Union Medical College Hospital for her cooridnation work.

Authors' contributions

QL(Qiaofei Liu), QL, HZ, and YZ conceived the idea. HZ, QL (Qiaofei Liu), NH, SY, XL, and JL conducted experiments, collected the data, and analyzed the data. HZ draw all the figures and tables and prepared all the supplementary materials. XY, YY, QJ, YJ, and SW produced the CAR-c-MET-hMDM cells and conducted experiments. QL（Qiaofei Liu）, HZ, and XY wrote and revised this manuscript. JK dicussedthe data, gave critical comments and revised the manuscript. All of the authors approved the submission to this journal.

Funding

This study was supported by the Natural Science Foundation of China (82373230,8237101375), CAMS Innovation Fund for Medical Sciences(2023-I2M-C&T-B-024), National High-Level Hospital Clinical Research Funding (2022-PUMCH-D-001).

Data availability

No datasets were generated or analysed during the current study.

Declarations

Ethics approval and consent to participate

The Institutional Review Board of Peking Union Medical College Hospital approved this animal study (February 15th, 2023, XHDW-2022–126). Human blood for this study was ethically sourced and analyzed with approval from the Roc Rock Biotechnology Ethics Committee (approval number 2022,002). Research adhered to medical standards and regulations.

Competing interests

The authors declare no competing interests.

Author details

[1]Department of General Surgery, State Key Laboratory of Complex Severe and Rare Diseases, Dongcheng District, Peking Union Medical College Hospital, Peking Union Medical College, Chinese Academy of Medical Sciences, No.1 Shuai Fu Yuan, Beijing 100730, China. [2]Medical Research Center, State Key Laboratory of Complex Severe and Rare Diseases, Dongcheng District, Peking Union Medical College Hospital, Peking Union Medical College, Chinese Academy of Medical Sciences, No.1 Shuai Fu Yuan, Beijing 100730, China. [3]Applied Biology Laboratory, College of Pharmaceutical and Biological Engineering, Shenyang University of Chemical Technology, Shenyang 110142, China. [4]Roc Rock Biotechnology (Shenzhen), Shenzhen 518118, China. [5]Department of Visceral, Vascular and Endocrine Surgery, Martin-Luther-University Halle-Wittenberg, 06120 Halle (Saale), Germany.

Received: 2 May 2024 Accepted: 23 November 2024
Published online: 06 December 2024

References

1. Bray, F., et al., Global cancer statistics 2022: GLOBOCAN estimates of incidence and mortality worldwide for 36 cancers in 185 countries. CA Cancer J Clin, 2024.
2. Zhao Y, et al. Chinese expert consensus on minimally invasive radical surgery for pancreatic ductal adenocarcinoma (version 2022). Journal of Pancreatology. 2022;5(3):111–7.
3. Wu W, et al. Real-world study of surgical treatment of pancreatic cancer in China: annual report of China Pancreas Data Center (2016–2020). Journal of Pancreatology. 2022;5(1):1–9.
4. Conroy T, et al. FOLFIRINOX versus gemcitabine for metastatic pancreatic cancer. N Engl J Med. 2011;364(19):1817–25.

5. Xu ZH, et al. Insight of pancreatic cancer: recommendations for improving its therapeutic efficacy in the next decade. Journal of Pancreatology. 2022;5(2):58–68.
6. Caronni N, et al. IL-1beta(+) macrophages fuel pathogenic inflammation in pancreatic cancer. Nature. 2023;623(7986):415–22.
7. Liu Q, et al. Adoptive cellular immunotherapy for solid neoplasms beyond CAR-T. Mol Cancer. 2023;22(1):28.
8. Liu Q, et al. Combined blockade of TGf-beta1 and GM-CSF improves chemotherapeutic effects for pancreatic cancer by modulating tumor microenvironment. Cancer Immunol Immunother. 2020;69(8):1477–92.
9. Yang S, Liu Q, Liao Q. Tumor-Associated Macrophages in Pancreatic Ductal Adenocarcinoma: Origin, Polarization, Function, and Reprogramming. Front Cell Dev Biol. 2020;8: 607209.
10. Liu Q, Liao Q, Zhao Y. Chemotherapy and tumor microenvironment of pancreatic cancer. Cancer Cell Int. 2017;17:68.
11. Deng Z, et al. The nuclear factor ID3 endows macrophages with a potent anti-tumour activity. Nature. 2024;626(8000):864–73.
12. Nywening TM, et al. Targeting tumour-associated macrophages with CCR2 inhibition in combination with FOLFIRINOX in patients with borderline resectable and locally advanced pancreatic cancer: a single-centre, open-label, dose-finding, non-randomised, phase 1b trial. Lancet Oncol. 2016;17(5):651–62.
13. Gomez-Roca, C., et al., Anti-CSF-1R emactuzumab in combination with anti-PD-L1 atezolizumab in advanced solid tumor patients naive or experienced for immune checkpoint blockade. J Immunother Cancer, 2022. 10(5).
14. Klichinsky M, et al. Human chimeric antigen receptor macrophages for cancer immunotherapy. Nat Biotechnol. 2020;38(8):947–53.
15. Luna J, et al. DYRK1A modulates c-MET in pancreatic ductal adenocarcinoma to drive tumour growth. Gut. 2019;68(8):1465–76.
16. Mekapogu AR, et al. HGF/c-Met pathway inhibition combined with chemotherapy increases cytotoxic T-cell infiltration and inhibits pancreatic tumour growth and metastasis. Cancer Lett. 2023;568: 216286.
17. Mori S, et al. Inhibition of c-MET reverses radiation-induced malignant potential in pancreatic cancer. Cancer Lett. 2021;512:51–9.
18. Mohd Yasin ZN, et al. Macrophage polarization in THP-1 cell line and primary monocytes: A systematic review. Differentiation. 2022;128:67–82.
19. Qi, C., et al., CT041 CAR T cell therapy for Claudin18.2-positive metastatic pancreatic cancer. J Hematol Oncol, 2023. 16(1): p. 102.
20. Feng K, et al. Phase I study of chimeric antigen receptor modified T cells in treating HER2-positive advanced biliary tract cancers and pancreatic cancers. Protein Cell. 2018;9(10):838–47.
21. Lee HH, et al. Therapeutic effiacy of T cells expressing chimeric antigen receptor derived from a mesothelin-specific scFv in orthotopic human pancreatic cancer animal models. Neoplasia. 2022;24(2):98–108.
22. Faradji A, et al. Phase I study of liposomal MTP-PE-activated autologous monocytes administered intraperitoneally to patients with peritoneal carcinomatosis. J Clin Oncol. 1991;9(7):1251–60.
23. Lopez, M., et al., Adoptive immunotherapy with activated macrophages grown in vitro from blood monocytes in cancer patients: a pilot study. J Immunother (1991), 1992. 11(3): p. 209–17.
24. Andreesen R, Hennemann B, Krause SW. Adoptive immunotherapy of cancer using monocyte-derived macrophages: rationale, current status, and perspectives. J Leukoc Biol. 1998;64(4):419–26.
25. Pan, Q., et al., Chimeric Antigen Receptor Macrophages Target and Resorb Amyloid Plaques in a Mouse Model of Alzheimer's Disease. bioRxiv, 2023.
26. Duan Z, et al. Chimeric antigen receptor macrophages activated through TLR4 or IFN-gamma receptors suppress breast cancer growth by targeting VEGFR2. Cancer Immunol Immunother. 2023;72(10):3243–57.
27. Hu X, et al. Safety, efficacy and pharmacokinetics of BPI-9016M in c-MET overexpression or MET exon 14 skipping mutation patients with locally advanced or metastatic non-small-cell lung cancer: a phase Ib study. BMC Cancer. 2023;23(1):331.
28. Zhang W, et al. Chimeric antigen receptor macrophage therapy for breast tumours mediated by targeting the tumour extracellular matrix. Br J Cancer. 2019;121(10):837–45.
29. Camidge DR, et al. Phase I Study of 2- or 3-Week Dosing of Telisotuzumab Vedotin, an Antibody-Drug Conjugate Targeting c-Met, Monotherapy in Patients with Advanced Non-Small Cell Lung Carcinoma. Clin Cancer Res. 2021;27(21):5781–92.
30. Camidge DR, et al. Phase Ib Study of Telisotuzumab Vedotin in Combination With Erlotinib in Patients With c-Met Protein-Expressing Non-Small-Cell Lung Cancer. J Clin Oncol. 2023;41(5):1105–15.
31. Huo Y, et al. M1 polarization enhances the antitumor activity of chimeric antigen receptor macrophages in solid tumors. J Transl Med. 2023;21(1):225.
32. Wang C, Wu Y, Wang W. Neoadjuvant therapy for resectable pancreatic cancer: a narrative review. Journal of Pancreatology. 2022;5(2):69–77.
33. Halbrook CJ, et al. Pancreatic cancer: Advances and challenges. Cell. 2023;186(8):1729–54.
34. Pan, K.,et al., CAR race to cancer immunotherapy: from CAR T, CAR NK to CAR macrophage therapy. Journal of experimental & clinical cancer research ,2022. CR, 41(1), 119.
35. Li J, Chen P, Ma W. The next frontier in immunotherapy: potential and challenges of CAR-macrophages. Exp Hematol Oncol. 2024;13(1):76.
36. Li N, Geng S, Dong ZZ, et al. A new era of cancer immunotherapy: combining revolutionary technologies for enhanced CAR-M therapy. Mol Cancer. 2024;23(1):117.
37. Sloas C, Gill S, Klichinsky M. Engineered CAR-Macrophages as Adoptive Immunotherapies for Solid Tumors. Front Immunol. 2021;12: 783305.
38. Schepisi G, Gianni C, Palleschi M, et al. The New Frontier of Immunotherapy: Chimeric Antigen Receptor T (CAR-T) Cell and Macrophage (CAR-M) Therapy against Breast Cancer. Cancers (Basel). 2023;15(5):1597.

Publisher's Note